ORNL/TM-2022/ 2517

An Extrapolation Method for Strain Ranges and Hold Times in Developing the EPP+SMT Creep-Fatigue Design Curves for Alloy 617

Yanli Wang
Peijun Hou
T.-L. Sham

July 2022

OAK RIDGE National Laboratory

ORNL IS MANAGED BY UT-BATTELLE LLC FOR THE US DEPARTMENT OF ENERGY

ORNL/TM-2022/ 2517

Materials Science and Technology Division

AN EXTRAPOLATION METHOD FOR STRAIN RANGES AND HOLD TIMES IN DEVELOPING THE EPP+SMT CREEP-FATIGUE DESIGN CURVES FOR ALLOY 617

Yanli Wang
Peijun Hou[1]
T.-L. Sham[2]

[1] Imtech Corporation, Knoxville
[2] Idaho National Laboratory

Date Published: July 2022

Prepared by
OAK RIDGE NATIONAL LABORATORY
Oak Ridge, TN 37831
managed by
UT-BATTELLE LLC
for the
US DEPARTMENT OF ENERGY
under contract DE-AC05-00OR22725

CONTENTS

LIST OF FIGURES

LIST OF TABLES

ABBREVIATIONS

ART	Advanced Reactor Technologies
ASME	American Society of Mechanical Engineers
CF	creep-fatigue
DOE	US Department of Energy
EPP	elastic-perfectly plastic
INL	Idaho National Laboratory
ORNL	Oak Ridge National Laboratory
SBSMT	single-bar simplified model test
SMT	simplified model test

ACKNOWLEDGMENTS

This research was sponsored by the US Department of Energy (DOE) under contract no. DE-AC07-05ID14517 with Idaho National Laboratory, managed and operated by Battelle Energy Alliance; and under contract no. DE-AC05-00OR22725 with Oak Ridge National Laboratory (ORNL), managed and operated by UT-Battelle LLC. Programmatic direction was provided by the Office of Nuclear Reactor Deployment of the DOE Office of Nuclear Energy.

The authors gratefully acknowledge the support provided by Sue Lesica, Federal Materials Lead for the Advanced Reactor Technologies (ART) Program; Matthew Hahn, Federal Program Manager of the ART Gas-Cooled Reactors (GCR) Campaign; and Gerhard Strydom of Idaho National Laboratory, National Technical Director of the ART GCR Campaign.

The authors also wish to thank ORNL staff members C. Shane Hawkins for technical support and Lianshan Lin and Jian Chen for reviewing this report.

ABSTRACT

Experimental and numerical studies in developing the integrated Elastic–Perfectly Plastic (EPP) plus Simplified Model Test (SMT) design methodology, referred to as the *EPP+SMT method*, continued in FY2022. This report focuses on the methods for extrapolating the EPP+SMT creep-fatigue (CF) design curves at long hold times and low strain ranges.

In this study, the available CF failure data on Alloy 617 at 950 ºC were analyzed to determine a set of CF failure criteria. At very low strain ranges and long hold times, CF failure data are not accessible by experiments because of the extraordinarily long test durations and the inability of the test machines to accurately control these small strain ranges. A CF experimental approach with the concept of block-strain range CF testing protocol was developed. Tests using this protocol were conducted to generate the needed information for calibrating material parameters of the numerical material models. The Time Fraction based method and Dissipated Energy method were used to extrapolate the CF life curves to low strain ranges and long hold times. Based on the new experimental approach and CF life prediction methods, the CF life curves with various hold times were developed for Alloy 617 at 950°C. In addition, an experiment was designed and is being performed to verify the predicted CF curves at 950°C.

The extrapolation procedure will be applied at lower temperatures to complete the development of the EPP+SMT CF design curves for Alloy 617 in F2023.

1. BACKGROUND

Creep-fatigue (CF) interactive damage to structural components under cyclic loading at elevated temperatures is much more deleterious than pure fatigue or pure creep damage mode. In the last 40 years, significant efforts have been devoted to elevated temperature code rule development in the American Society of Mechanical Engineers (ASME) *Boiler and Pressure Vessel Code* (Section III, Division 5, Subsection HB, Subpart B) to ascertain conservative structural designs against CF failure. The current Subsection HB, Subpart B CF evaluation in the design procedure was established by (1) analytically obtaining a detailed stress-strain history, (2) comparing the stress and strain components with cyclic test results and deconstructing into stress and strain quantities to evaluate the creep damage and fatigue damage separately, and (3) recombining the results to obtain a damage function in the form of the CF damage diagram. The deconstruction and recombination of the stress and strain quantities present difficulties in evaluating test data and determining cyclic damage in design. The uncertainties in these steps lead to the use of the overly conservative approaches in the current CF design procedure.

The integrated Elastic–Perfectly Plastic (EPP) plus Simplified Model Test (SMT) design methodology, referred to as the *EPP+SMT method*, is an alternative CF evaluation methodology. The concept is to incorporate the SMT CF test data-based approach into the EPP methodology to avoid evaluating creep and fatigue damage separately. This approach greatly simplifies the evaluation procedure for elevated temperature cyclic service. In this SMT-based approach, the key feature is that it no longer requires the damage interaction, or damage diagram, and the combined effects of creep and fatigue are accounted for in the SMT test data. The SMT specimens are designed to replicate or bound the stress and strain redistribution that occurs in actual components when loaded in the creep regime. On the other hand, the EPP methods greatly simplify the design evaluation procedure by eliminating the need for stress classification, which is the basis of the current simplified design rules. The goal of this EPP+SMT methodology is to maximize the advantages of EPP methods and the SMT CF evaluation approach. Also, the EPP+SMT method aims to release the conservatism in the existing CF evaluation procedure while properly accounting for enhanced creep damage around localized defects and stress risers.

A detailed plan was developed and subsequently revised for the development of this EPP+SMT methodology (Wang et al. 2016a, 2016b, 2017a, 2018, 2019; Messner 2018). The development of SMT-based design curves requires experimental data, and the parameters to be considered include elastic follow-up factor, strain range, loading/straining rate, test temperature, hold time, and primary load. In the original SMT key feature testing methods, the elastic follow-up factor was achieved by sizing the length and area ratios of the driver section to the test section. Achieving the requisite representation of creep damage characteristics via key featured SMT, particularly at very high temperatures, involves specimen configurations that are both costly and beyond the limits of test control and stability (Wang et al. 2013, 2014, 2015, 2016a, 2017b, 2017c). Although key featured SMT testing is crucial in verifying the SMT-based design methodology, it is impractical for use in generating data for SMT-based design curves.

Wang et al. made significant progress in developing SMT experimental techniques (2018, 2019, 2020). In particular, the newly developed single-bar SMT (SBSMT) test method and test protocol overcame many challenges associated with SMT key feature experiments and enabled evaluation of the effect of elastic follow-up by using a standard CF specimen without specialized instrumentation and specimen design. In FY2019, Wang et al. (2019) demonstrated the SBSMT method on Alloy 617, SS316H, and Grade 91 by testing at high temperatures and successfully showed the flexibility of generating SMT-based failure data with a wide range of elastic follow-up values from 1 to 12. In FY2022, Idaho National Laboratory (INL) applied the SBSMT method using software feedback control (Wang, 2022). The SBSMT test method significantly simplifies the procedure for generating SMT test data and allows SMT-based design method development to advance rapidly.

In FY2020, Wang et al. (2020, 2021) extended the SBSMT method to internal pressurized tubular specimens at 950°C on Alloy 617. The sustained primary load was introduced by the internal pressure. The test results from this study along with the original SMT data on Alloy 617, demonstrated that although internal pressure is within the allowable stress limit per ASME Section III, Division 5, Code Case N-898, the SMT CF cycles to failure were reduced for the cases tested with primary-pressure load. The reduction of SMT CF life because of primary load was found to be dependent on strain ranges and elastic follow-up factors. Approaches to account for the primary-load effect on SMT design curves were discussed in Barua et al. (2020, 2021), and the results show that the EPP strain range analysis procedure naturally captures the primary pressure effect. Barua et al. (2020, 2021) also demonstrated that the EPP+SMT methodology is much simpler to execute than conventional CF damage analyses through multiple sample problems.

The remaining critical factors in finalizing the SMT-based design curves are the methods for extrapolating the design curves to the low strain range region and with longer hold times (such as long hold time of 1,000 h) that are prototypical of plant operations. In this report, strain-controlled standard CF test data and SMT CF test data are used to assess CF damage. A specially designed experimental approach with the concept of block-strain range CF testing protocol was developed and tests using this protocol were conducted on Alloy 617 at 950°C to obtain critical information in extrapolating CF life curves to low strain ranges and long hold times. In addition, an experiment was designed and is being performed to generate data to verify the predicted CF curves. The analysis and results provide general guidance on the development of CF design curves.

2. MATERIAL AND EXPERIMETAL

2.1 ALLOY 617 MATERIAL AND CREEP-FATIGUE EXPERIMETS

The Alloy 617 specimens were machined from the Alloy 617 plate with heat number 314626 from ThyssenKrupp VDM USA Inc, supplied to support this research by the INL. The plate has a nominal thickness of 38 mm. The chemical composition of the plate is listed in Table 1.

Table 1. Chemical compositions of Alloy 617 plate with heat number 314626 (wt%)

C	S	Cr	Ni	Mn	Si	Mo	Ti	Cu	Fe	Al	Co	B
0.05	<0.002	22.2	54.1	0.1	0.1	8.6	0.4	0.04	1.6	1.1	11.6	<0.001

The specimen geometry used in this report for experimental CF tests is shown in Figure 1. The specimen has a gage diameter of 6.35 mm and a gage length of 19.05 mm. The CF testing procedure followed ASTM E2714-13 standard (ASTM 2013) under strain-controlled mode. The specimen longitudinal direction is oriented along the rolling direction of the material plate. All the specimens were tested in the as-received, solution-annealed condition.

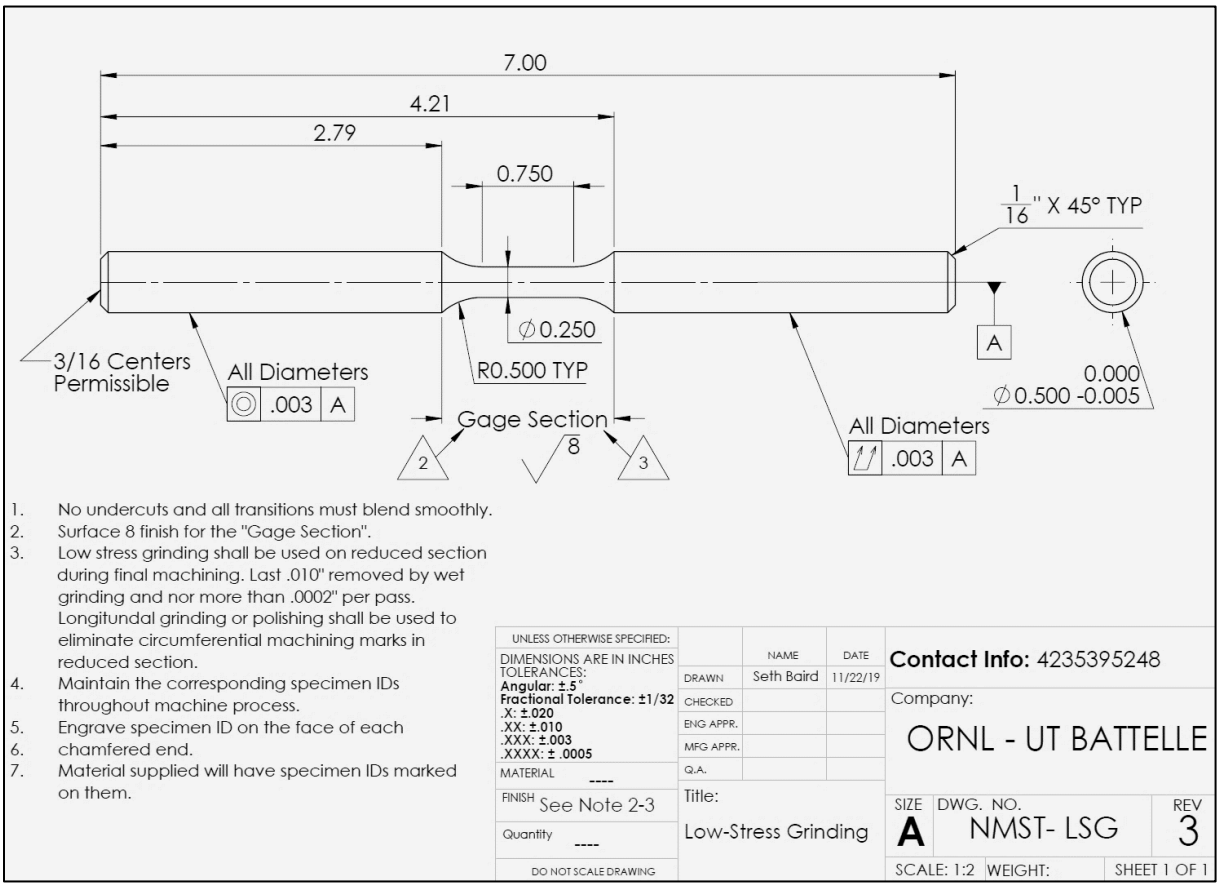

Figure 1. Standard fatigue and CF specimen geometry at Oak Ridge National Laboratory (dimensions are in inches).

The straining profile for standard strain-controlled CF is shown schematically in Figure 2. The hold-time segment is applied to the maximum tensile strain amplitude for CF testing. The straining profile is a fully reversed profile (i.e., with a nominal straining ratio of R = -1). The nominal strain rate is 1E-3/s. The control extensometer has a nominal gage length of 12.7 mm.

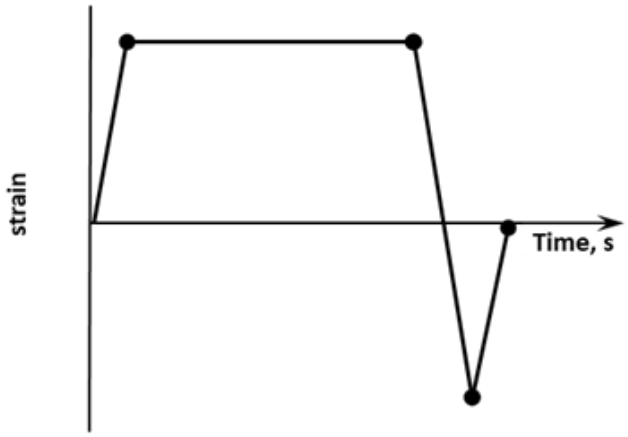

Figure 2. Strain-controlled CF straining profile for one cycle.

Previous SMT-based CF test results at low strain ranges at 950°C on the same heat of Alloy 617 plate (heat 314626) were analyzed in the this report. The details of the experimental procedure are explained in the previous reports (Wang et al. 2022, 2021, 2020, 2019, 2018, 2016a, 2013).

There is an ongoing SBSMT test with an elastic follow-up factor of 3 on Alloy 617 at 950°C to verify the results of CF cyclic life prediction. The test specimen geometry and the test setup are the same as the standard CF test. The details of achieving the elastic follow-up factor using the standard CF test setup are explained in Wang et al. 2019.

2.2 AVAILABLE CREEP-FATIGUE FAILURE DATA

The tensile-hold CF tests with failure information conducted at Oak Ridge National Laboratory (ORNL) and INL at higher strain ranges and shorter hold times are collected as a baseline study in this report. The collected CF data are summarized in Table 2.

Note that the standard and SMT creep-fatigue experiments were carried out under the uniaxial loading condition, although the SMT-based design methodology can be applied to multiaxial states through equivalent strain range and equivalent stress measures. More details on the experiments and material including the specimen dimension, strain rate, and microstructural information of the plate can be found in previous reports (Wang et al. 2021, Wright et al. 2016).

Table 2. Summary of the tensile-hold creep-fatigue testing results of Alloy 617 at 950ºC.

Data source	Specimen ID	Elastic follow-up factor	Strain range (%)	Tensile hold time (s)	Cycle to failure
INL	A-6	1	1.0	180	350
	F-5	1	1.0	180	450
	A-13	1	1.0	600	300
	E-1	1	1.0	600	400
	E-8	1	1.0	600	400
	F-4	1	1.0	600	400
	E-7	1	1.0	1800	350
	E-9	1	1.0	1800	350
	E-10	1	1.0	9000	350
	A-23	1	0.6	180	949
	A-14	1	0.6	600	550
	B-18	1	0.6	600	700
	B-19	1	0.6	600	600
	B-21	1	0.6	1800	650
	B-5	1	0.3	180	3899
	B-6	1	0.3	180	2399
	A-22	1	0.3	600	4399
	B-7	1	0.3	600	3999
	B-9	1	0.3	600	2599
	B-8	1	0.3	1800	4599
	B-11	1	0.3	1800	4799
ORNL	R13TC6	1	0.17	120	64659
	SBA7-P20	2	0.25	600	3224
	R12TC4-05	3	0.18	600	5363

2.3 SPECIFICIALY DESIGNED BLOCK-STRAIN RANGE CF TESTING

In supporting of extrapolating the CF life curves to long hold times and low strain ranges, CF experiments are designed to collect the key experimental information by applying a series of CF loading blocks (i.e., with variations of strain ranges and hold times) on a single specimen with a certain number of applied cycles. The testing conditions are listed in Table 3.

Figure 3 shows the maximum and minimum stresses of the specially designed block-strain range CF tests. The results with a 100 s tensile hold time, in Figure 3a, show that the maximum stresses at different strain ranges gradually approach the same values with increasing cycle numbers. Figure 3b and 3c show that the maximum stresses at different strain ranges with 1,000 s or 10,000 s hold times become almost the same after a few cycles, although the minimum stresses decrease with applied strain range.

The results indicate that the stress relaxation process follow almost the same curves when the applied strain range is from 0.17% to 0.07%, resulting in similar creep damage at such strain ranges. Tests with longer hold times approach the same values with less applied cycles.

Table 3. Specially designed block-strain range creep-fatigue testing on Alloy 617 at 950°C.

Block-strain ID	Nominal strain range (%)	Tensile hold time (s)
1	0.17	100
2	0.15	100
3	0.13	100
4	0.09	100
5	0.07	100
6	0.17	1,000
7	0.15	1,000
8	0.13	1,000
9	0.09	1,000
10	0.07	1,000
11	0.17	10,000
12	0.13	10,000
13	0.09	10,000
14	0.07	10,000
15	0.3	360,000
16	0.05	360,000

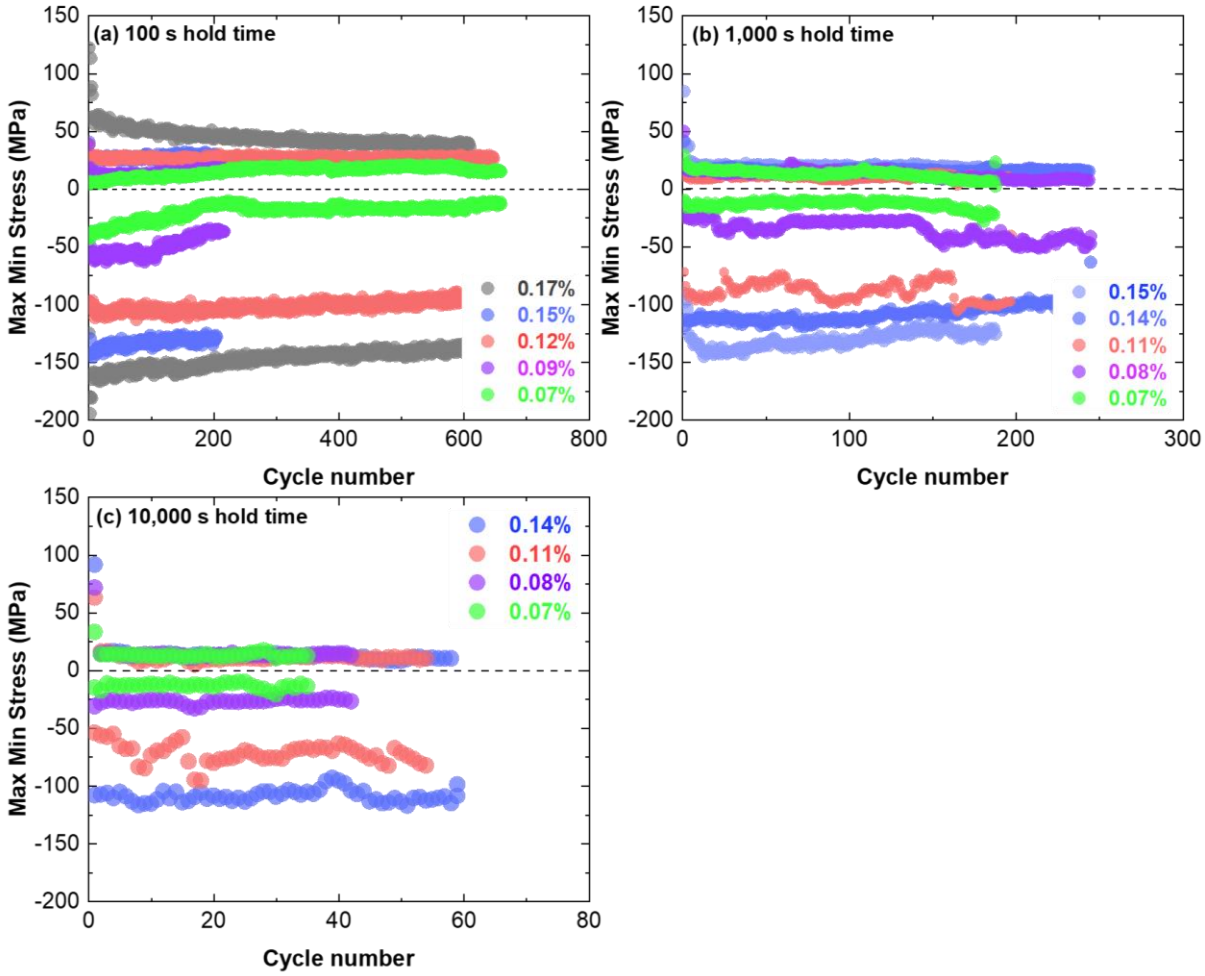

Figure 3. Maximum and minimum stresses as a function of applied cycles of the specially designed block-strain range CF tests.

3. EXTRAPOLATING CREEP-FATIGUE DATA

3.1 EXTRAPOLATING STRESS RELAXATION CURVES TO LONG HOLD TIMES

The available CF failure data are limited to tests with short hold time of 0.5 h and less, and only very few tests with the hold times longer than 1 h were tested to failure. It is not practical to perform experiments to failure with much longer hold time. For example, a test with 100 h hold for 100 cycles at 1% strain range will last for ~14 months. Extrapolation methods are needed for generating CF life curves with long hold times that are representative to typical operation hold time of 1,000 h.

An accurate description of the stress relaxation behavior during hold time for strain-controlled tests is essential for evaluation of the creep damage during cyclic loading. In this study, a classical elastic, rate-independent plastic, and creep viscoplasticity model is adopted to extrapolate the stress relaxation to long hold times. From the basic elastic, rate-independent plastic, creep model, the total strain rate $\dot{\varepsilon}$ under a uniaxial loading condition can be decomposed and expressed as

$$\dot{\varepsilon} = \dot{\varepsilon}_e + \dot{\varepsilon}_p + \dot{\varepsilon}_c \tag{1}$$

where $\dot{\varepsilon}_e$, $\dot{\varepsilon}_p$, and $\dot{\varepsilon}_c$ denote elastic strain rate, plastic strain rate, and creep strain rate, respectively. During the tensile hold period under strain-controlled mode, $\dot{\varepsilon} = \dot{\varepsilon}_p = 0$. Expressing the elastic strain rate as $(\dot{\sigma}/E)$, where $\dot{\sigma}$ is the stress rate, and E is the Young's modulus, Eq.1 can be rewritten to describe the stress relaxation as

$$\frac{\dot{\sigma}}{E} + \dot{\varepsilon}_c = 0 \tag{2}$$

Moreover, the effect of elastic follow-up is an important factor for design of structural components at elevated temperatures, and its detrimental effects on the components' life were discussed in detail in Wang et al. (2017, 2018, 2019). The enhanced creep damage accumulation and retarded stress relaxation due to the elastic follow-up will need to be accounted for. In this work, the influence of elastic follow-up factor, q, on the stress relaxation process is described as follows (Kobatake et al. 1999)

$$\frac{\dot{\sigma}}{E} + \frac{1}{q}\dot{\varepsilon}_c = 0 \tag{3}$$

For standard CF tests under strain-controlled mode, $q = 1$, and Eq. 3 is reduced to Eq. 2.

To describe the stress relaxation behavior, Eq. 4 is used to implement the relationship between $\dot{\varepsilon}_c$ and σ as follows (Cocks et al. 1982):

$$\frac{1}{\dot{\varepsilon}_0}\dot{\varepsilon}_c = A\left(\frac{\sigma}{\sigma_0}\right) + B\left(\frac{\sigma}{\sigma_0}\right)^n \tag{4}$$

where, A is the coefficient for grain boundary diffusion, B is the coefficient for power-law creep, $\dot{\varepsilon}_0$ denotes the initial creep strain rate, σ_0 is the reference stress, and n is the stress exponent. In this report, two evaluation methods, i.e., the Time Fraction based method and Dissipated Energy method, are used to assess creep damage during the tensile hold segment. The details of the coefficients and the material parameters in the coefficient A and B for these two evaluation methods are described in *Section 4* of this report.

It is assumed that there is no threshold stress in Eq. 4 for Alloy 617 at 950 °C. In this study, by substituting the creep strain rate $\dot{\varepsilon}_c$ in Eq. 3 using Eq. 4, the experimental stress relaxation curves during tensile hold are fitted, with $\dot{\varepsilon}_0$ and σ_0 being the fitting parameters, for every cycle of all available test data. In the analysis, the creep damage in the subsequent cycles is calculated based on the fitted stress relaxation curve. When extrapolating the stress relaxation curves to longer hold times or low strain ranges using the viscoplasticity model, the effect of hold time on the initial stresses at the start of the hold time was neglected, and the $\dot{\varepsilon}_0$ and σ_0 were set to be the average values of what were used for fitting the experimental data. The $\dot{\varepsilon}_0$ and σ_0 values used in the viscoplasticity model are listed in Table 5 of this report. The stress exponent, n, in the power-law creep relation is set to be 5.6 for Alloy 617 at 950 °C (Benz et al. 2014).

3.2 EXTRAPOLATING DATA AT LOW STRAIN RANGE

To generate experimental CF failure data at very low strain ranges has similar issue of extreme long test duration. For example, at strain range of 0.2%, a CF test with 0.5 h hold time is estimated to last 7 months at 950 °C, and the test duration would be much longer when hold time is increased. Further, the high noise-to-signal ratio also creates additional uncertainty for strain-controlled tests at low strain ranges. To study the mechanical response of materials subject to cyclic loading at low strain ranges, numerical modeling is needed.

In this report, a classical elastic, plastic, and creep model is adopted to simulate the mechanical response, especially at low strain ranges, as explained above. The plastic strain and creep strain in Eq. 1 are decoupled and considered separately in this plasticity-creep partition model.

For the elastic strain rate, the standard linear elastic constitutive equation for an isotropic material is applied.

$$d\varepsilon_{ij}^{e} = D_{ijkl} : d\sigma_{kl} \tag{5}$$

where D_{ijkl} is the elastic compliance tensor. The Von Mises yield criterion is used to simulate the rate-independent plastic flow, and it is defined as the condition when

$$f(\sigma_{ij}, \alpha_{ij}, R) = \sqrt{\frac{3}{2}(S_{ij} - \alpha_{ij}) : (S_{ij} - \alpha_{ij})} - R(\bar{\varepsilon}^{p}) = 0 \tag{6}$$

where S_{ij} is the component of the deviatoric stress tensor and given by $S_{ij} = \sigma_{ij} - \frac{1}{3}\sigma_{kk}\delta_{ij}$, α_{ij} is the back stress, and R denotes the deformation resistance. The accumulated plastic strain, $\bar{\varepsilon}^{p}$, is determined from the condition where the Von Mises yield criterion is satisfied, and the increment of the equivalent plastic strain, $d\varepsilon_{ij}^{p}$, is

$$d\bar{\varepsilon}^{p} = \sqrt{\frac{2}{3} d\varepsilon_{ij}^{p} : d\varepsilon_{ij}^{p}} \tag{7}$$

Based on the study on CF damage (Zhao et al. 2019), a modified power-law isotropic hardening model (Eq. 8) and the Armstrong-Frederick kinematic hardening model (Eq. 9) are used to describe the hardening behavior (Chaboche 1989, Zhao et al. 2019, Li et al. 2020),

$$R = \left(\sigma_{oY} + h|\bar{\varepsilon}^p|^{\eta} + Q_0\left(1 - e^{-b|\bar{\varepsilon}^p|}\right)\right)\left(1 - \frac{dD^{TF}}{dN}\right)^{\varphi} \quad (8)$$

where σ_{oY} is the initial cyclic yield stress, Q_0 and b describe the first stage of cyclic softening, h and η are the material parameters related to the slope of softening stage, φ is the material parameter related to the influence of CF damage on cyclic stress softening, D^{TF} denotes accumulated CF damage (in Eq. 20), and N is cycle number. The details of the CF damage evaluation are provided in *Section 4*. It is assumed that the accumulated CF damage would cause material softening during cyclic loading for Alloy 617 at 950°C, so that the CF damage term is added to the yield surface (Eq. 8) to represent the resultant softening effect.

$$d\alpha_{ij} = \frac{2}{3}c_0 d\varepsilon_{ij}^p - \gamma\alpha_{ij}d\bar{\varepsilon}^p \quad (9)$$

where c_0 is the kinematic hardening rate, and γ represents the model parameter of the recovery item. $\gamma = 0$ stands for the linear kinematic hardening rule. The material parameters are calibrated using the experimental CF results and are listed in Table 4.

The relationship between creep strain rate, $\frac{d\varepsilon_c}{dt}$, and stress in this numerical model is described using Cocks-Ashby model (Cocks et al. 1982). In this report, we refer Cocks-Ashby model as Creep Cavity Growth model. The details of this model will be provided in *Section 4.1* of this report.

Table 4. Material parameters in the viscoplasticity model of Alloy 617 at 950°C.

Parameters	Value
E	136 GPa
σ_{oY}	155 MPa
h	-0.1 MPa
η	1
Q_0	-23.5 MPa
b	4.2
c_0	25110 MPa
γ	620 MPa
φ	0.15

4. DAMAGE ANALYSIS METHODOLOGY

In this section, two methods for creep damage assessment, i.e., Time Fraction based method and Dissipated Energy method, are introduced and discussed. These two methods are briefly outlined in the following.

4.1 TIME FRACTION

The CF evaluation procedure in Section III, Division 5 of the ASME Boiler and Pressure Vessel Code uses the Time Fraction method for creep damage evaluation. In this method, the stress is regarded as the key parameter controlling the creep damage. In literature, many models have been developed to correlate creep rupture time with applied stress. For example, the Larson-Miller relationship was used for Alloy 617 in Wright et al 2016. However, the Larson-Miller relationship is only valid to stress levels larger 11 MPa, for the small stress levels needed for the creep damage evaluation relevant to the low strain ranges, no valid relationship is available.

In this study, a Creep Cavity Growth model is used to describe the stress relaxation curves during CF testing, and for estimation of the creep rupture life. Cavities are assumed to grow by mechanisms such as grain-boundary diffusion, surface diffusion, and power-law dislocation creep in the grains. In this study, the Cocks-Ashby model (Cocks et al. 1982) was adopted, and the combination of grain-boundary diffusion and power-law creep is considered as the controlling mechanisms in the creep damage calculation. The creep damage is defined to be the growth of the cavities area fraction, f_h. The creep damage rate, $\frac{df_h}{dt}$, and the creep strain rate, $\frac{d\varepsilon_c}{dt}$, controlled by boundary diffusion mechanism are expressed as

$$\frac{1}{\dot{\varepsilon}_0}\frac{df_h}{dt} = \frac{\phi_0}{f_h^{1/2}\ln(1/f_h)}\left(\frac{\sigma}{\sigma_0}\right) \quad (10)$$

$$\frac{1}{\dot{\varepsilon}_0}\frac{d\varepsilon_c}{dt} = \frac{2\phi_0}{\ln(1/f_h)}\left(\frac{1}{d}\right)\left(\frac{\sigma}{\sigma_0}\right) \quad (11)$$

where d is the grain size, and the parameter ϕ_0 is given by

$$\phi_0 = \frac{2\pi D_B \delta_B \Omega}{kTl^3}\frac{\sigma}{\dot{\varepsilon}_0} \quad (12)$$

where $2l$ is the initial cavity spacing, D_B is the grain boundary diffusion rate, δ_B is the grain boundary thickness, Ω is the atomic volume, k is Boltzmann's constant, and T is absolute temperature.

The creep damage rate, $\frac{df_h}{dt}$, and the creep strain rate, $\frac{d\varepsilon_c}{dt}$, controlled by the power-law creep are expressed as

$$\frac{1}{\dot{\varepsilon}_0}\frac{df_h}{dt} = \beta\left[\frac{1}{(1-f_h)^n} - (1-f_h)\right]\left(\frac{\sigma}{\sigma_0}\right)^n \quad (13)$$

$$\frac{1}{\dot{\varepsilon}_0}\frac{d\varepsilon_c}{dt} = \left\{1 + \frac{2r_h}{d}\beta\left[\frac{1}{(1-f_h)^n} - 1\right]\right\}\left(\frac{\sigma}{\sigma_0}\right)^n \quad (14)$$

where $2r_h$ is the initial cavity diameter and the parameter β is given by

$$\beta = sinh\left[-2\frac{\left(n-\frac{1}{2}\right)}{\left(n+\frac{1}{2}\right)}\left(\frac{p}{\sigma}\right)\right] \quad (15)$$

where p is the hydrostatic pressure and is given by $p = -\frac{1}{3}\sigma$.

Implementing the creep damage rate and strain rate controlled by the combination of grain boundary diffusion and power-law creep with a linear summation on the above equations as

$$\frac{1}{\dot{\varepsilon}_0}\frac{df_h}{dt} = \frac{\phi_0}{f_h^{1/2}\ln(1/f_h)}\left(\frac{\sigma}{\sigma_0}\right) + \beta\left[\frac{1}{(1-f_h)^n} - (1-f_h)\right]\left(\frac{\sigma}{\sigma_0}\right)^n \quad (16)$$

$$\frac{1}{\dot{\varepsilon}_0}\frac{d\varepsilon_c}{dt} = \frac{2\phi_0}{\ln(1/f_h)}\left(\frac{1}{d}\right)\left(\frac{\sigma}{\sigma_0}\right) + \left\{1 + \frac{2r_h}{d}\beta\left[\frac{1}{(1-f_h)^n} - 1\right]\right\}\left(\frac{\sigma}{\sigma_0}\right)^n \quad (17)$$

In this Time Fraction method, Eq. 16 is used to calculate creep damage, and stress relaxation curve is described using Eq. 17. The accumulative creep damage from N cycles using this Time Fraction method is given as

$$D_c^{TF} = \sum_i^N f_h^i \quad (18)$$

where f_h^i is creep damage at cycle i.

Note that the equations in this section are modified to represent the case of uniaxial loading. However, the importance of the effects of multiaxial stress states in the creep cavitation was suggested by numerous studies (Sham et al. 1983, Wang et al. 2020). The analytical solutions in dealing with multiaxial stress states can be incorporated through equivalent strain range and equivalent stress measures. For example, in the Cocks-Ashby model, the creep failure can be assumed to be dependent on the equivalent stress (Von Mises stress, σ_e), the maximum principal stress, σ_1, and the hydrostatic pressure, p.

All the parameters in the Creep Cavity Growth model used in this report are list in Table 5. The initial cavity spacing, $2l$, is calibrated using creep rupture data of Alloy 617 at 950°C. The initial creep strain rate, $\dot{\varepsilon}_0$, and reference stress, σ_0 in power-law creep are calibrated using experimental relaxation curves. The stress exponent n in the power-law creep relation is set to be 5.6 and the grain size is assumed to be 150 micron (Benz et al. 2014). The parameters for boundary diffusion creep (i.e., boundary diffusion rate, D_B, boundary thickness, δ_B, and atomic volume, Ω) are available in Chapter 7 of Ref. Frost et al. (1982).

Table 5. Material parameters and typical stress relaxation fitting parameters used the Creep Cavity Growth model

Parameters in Creep Cavity Growth model	Value
Initial cavity spacing, $2l$	1.31×10^{-4} m
Initial cavity diameter, $2r_h$	5.52×10^{-7} m
Initial cavity area fraction, $f_{h,t=0}$	1.78×10^{-5}
Grain size, d	150×10^{-6} m
Boundary diffusion rate, D_B	115000 J/mol
Boundary thickness, δ_B	2.8×10^{-15} m^3/s
Atomic volume, Ω	1.1×10^{-29} m^3
Boltzmann's constant, k	1.38×10^{-23} J/K
Initial creep strain rate, $\dot{\varepsilon}_0$	4.5×10^{-5} /s
Stress exponent, n	5.6
Reference stress, σ_0	90 MPa

The creep rupture lives for Alloy 617 at 950°C were calculated using the Creep Cavity Growth model with the criterion to cause creep rupture being the case where the creep damage, f_h reaches 0.8. The creep rupture lives from the model are compared with the limited available creep rupture data from Wright et al (2022) in Figure 4, and the model reasonably represents the average creep strength of the available experimental data at 950 °C.

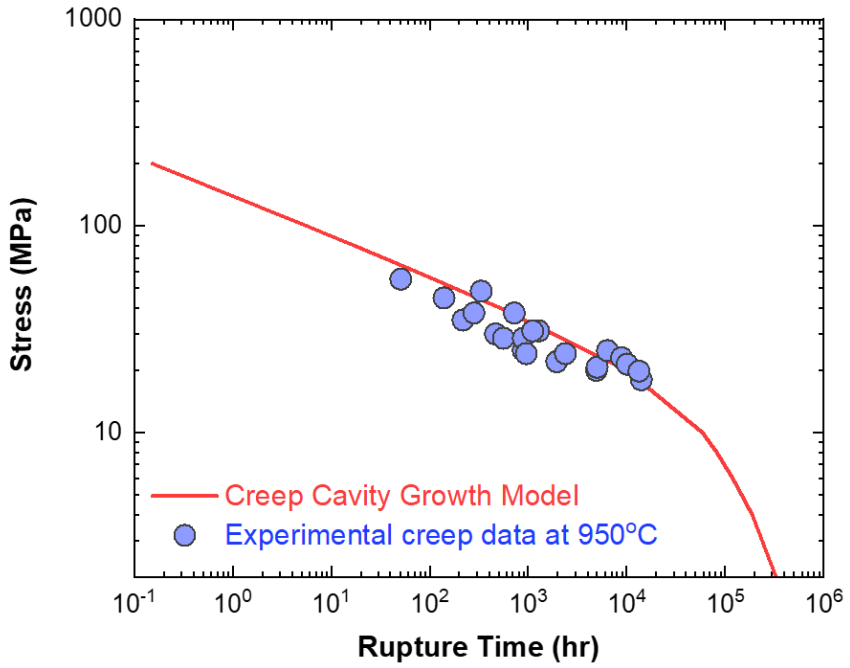

Figure 4. Comparison of the creep rupture predictions from the Creep Cavity Growth model with experimental data.

Generally, it is assumed that the fatigue life is related to the intrinsic ductility or Dissipated Energy in material. Based on Coffin-Manson Law and the Ostergren model (Ostergren 1976), a fatigue damage model used in this report is defined as follows

$$\frac{dD_f^{TF}}{dN} = \frac{\left(1 - D_f^{TF}\right)^{-\theta}}{\frac{1}{\beta} C_f \left|\sigma_{max} \Delta\varepsilon_p\right|^{-1/\beta}} \quad (19)$$

where D_f^{TF} is fatigue damage per cycle, N is cycle number, σ_{max} is the maximum stress per cycle, $\Delta\varepsilon_p$ is the plastic strain range, and α, θ, and C_f are material parameters. Table 6 lists the material parameters and their values in Eq. 19. The parameters α and θ are consistent with those in Zhao et al. (2019).

To assess the accumulative creep-fatigue damage and to predict creep-fatigue life using the Time Fraction, a nonlinear summation (Skelton et al. 2008, Zhao et al. 2019) is applied as

$$D^{TF} = \frac{D_c^{TF}}{1 - D_f^{TF}} + \frac{D_f^{TF}}{1 - D_c^{TF}} \quad (20)$$

where D^{TF} is the accumulated creep-fatigue damage, D_c^{TF} is accumulative creep damage, and D_f^{TF} is accumulative fatigue damage at cycle of N. The magnitude of D_c^{TF} and D_f^{TF} is set to be comparable by adjusting the material parameter, C_f in Eq. 19. The assumption is that creep-fatigue interaction is occurring when D_c^{TF} and D_f^{TF} have a similar magnitude of damage to the material under CF loading.

Furthermore, the influence of elastic follow-up on SMT CF life is assessed using Eqs. 3 and 4. Figure 5 shows an example from numerical simulation for SMT CF of 0.2% strain range and 600 s tensile hold with various elastic follow-up factors. Note that the retarded stress relaxation due to the increase of the elastic follow-up factor will induce higher creep damage, and thus a reduced CF life.

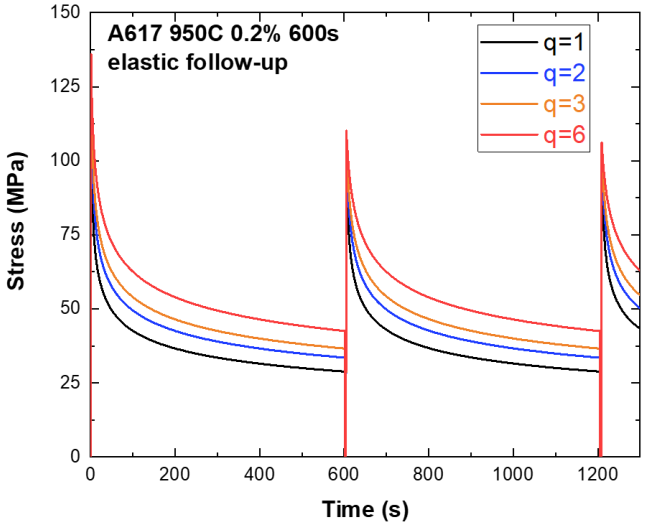

Figure 5. Relaxation curves using numerical simulation at 0.2% strain range and 600 s tensile hold with elastic follow-up factors of 1, 2, 3, and 6.

Table 6. Material parameters in the fatigue damage model used in Time Fraction method of Alloy 617 at 950°C.

Parameters	Value
β	0.84
θ	0.67
C_f	17,780 GPa

The analysis is performed on all the available standard and SMT-based CF data. In the study, the minimum value (i.e., 0.02) of the accumulated D^{TF} at failure from the available CF data is used as the failure criteria for CF life predictions. The results based on Time Fraction method are presented in *Section 5.1.1*.

It needs to point noted that

- there are very limited CF failure data in the literature available to support more comprehensive analysis, and there is no CF failure data below strain range of 0.17%;
- No clear trend on the critical CF damage values at failure could be identified from the limited CF failure data. In the CF life prediction study in this report, the lowest value of CF interactive damage (i.e., 0.02) obtained from all the available CF failure data is used as the failure criteria to determine the CF life cycles;
- At very low strain range of 0.02% and 0.01%, the lowest value of CF interactive damage (i.e., 0.02) is used to predict the CF life with 600 s tensile hold, and the CF cycles at 0.5hr, 1hr, 10hr, and 100 hr are computed by simply scaling the number of cycles at 600 s to the longer hold times, i.e., the cycles for a hold time of t_h is reduced by a factor of (t_h /600 s).

4.2 DISSIPATED ENERGY

Alternatively, the Dissipated Energy method has been developed with an assumption that the dissipated work (or strain energy) governs creep damage. In this method, the creep induced strain energy density at cycle i, d_c^i, is given by

$$d_c^i = \int_0^{t_h} \sigma \dot{\varepsilon}_c dt \quad (21)$$

And the creep strain energy density accumulated at cycle N, D_c^{SE}, is given by:

$$D_c^{SE} = \sum_i^N d_c^i \quad (22)$$

In this report, the experimental stress-strain hysteresis loop at each cycle is used to calculate the total dissipated work. The total dissipated work at cycle i can be decomposed into elastic, plastic, and creep part as

$$w_t^i = w_e^i + w_p^i + d_c^i = \int \sigma d\varepsilon_e + \int \sigma d\varepsilon_p + \int \sigma \dot{\varepsilon}_c dt \quad (23)$$

Then, fatigue damage at cycle i used in the analysis is computed by extracting the dissipated work induced by creep during the tensile hold (i.e., d_c^i) from the total dissipated work as

$$d_f^i = w_t^i - \int_0^{t_h} \sigma \dot{\varepsilon}_c \, dt \quad (24)$$

And the fatigue strain energy density accumulated at cycle N, D_f^{SE}, is given by:

$$D_f^{SE} = \sum_i^N d_f^i \quad (25)$$

The accumulated creep damage, D_c^{SE}, and accumulated fatigue damage, D_f^{SE}, are assessed separately on all the available standard CF and SMT-based CF data. D_c^{SE} values from all the test cycles are calculated by fitting the relaxation curve at each cycle, and the critical D_c^{SE} values at failure are determined as the creep failure criteria. The results will be presented in *Section 5.1.2*.

The hold time does not significantly affect the CF life because the changes in the stress rate or creep strain rate are extremely small when hold time exceeds a certain amount of period. In addition, studies indicate that the creep damage is the dominating factor at low strain ranges (Hales, 1980). Thus, in this study, only creep damage is analyzed to predict CF life at low strain ranges (i.e., strain range of 0.3% and less). The minimum value (the value of 150 mJ/mm^3 as explained in *Section 5.1.2*) of the accumulated D_c^{SE} at failure from the available data is used as the failure criteria for CF life predictions with longer hold times.

5. ANALYSIS AND RESULTS

5.1 DAMAGE ANALYSIS OF AVAILABLE CF FAILURE DATA

5.1.1 Damage Evolution Using Time Fraction Method

Standard CF test data with 120 s tensile hold at 0.18% strain range and SMT test data with 600 s tensile hold and elastic follow-up factors of 2 and 3 at strain ranges of 0.25% and 0.18%, are used to investigate creep damage, fatigue damage, and the CF interaction. Figure 6 shows the development of accumulated creep damage on these CF failure data as a function of applied cycle using the Time Fraction method. The stress relaxation curves in every cycle were fitted individually for creep damage calculation. The D_c^{TF} values at failure for the three experimental data are 0.014, 0.0014, and 0.0012, respectively. The accumulated creep damage is found to increase with the applied number with a linear relationship under log-log scale (i.e., a power-law relationship). This indicates the potential of predicting CF life using cyclic data with a limited number of cycles when a failure criterion or a critical damage value is determined.

Additionally, using standard CF test data with 0.18% and 1.0% strain range as an example, the creep damage, fatigue damage, and CF interactive damage calculated are presented in Figure 7. The creep damage, fatigue damage and CF interactive damage were all found to have a power-law relationship with the applied cycles. Extrapolations of the damages from the initial ~100 cycles with the simple power-law equations are also plotted as dashed lines in this figure to demonstrate this relationship. The analysis also shows that the role of creep damage or fatigue damage in CF interactive damage is dependent on both strain ranges and hold times.

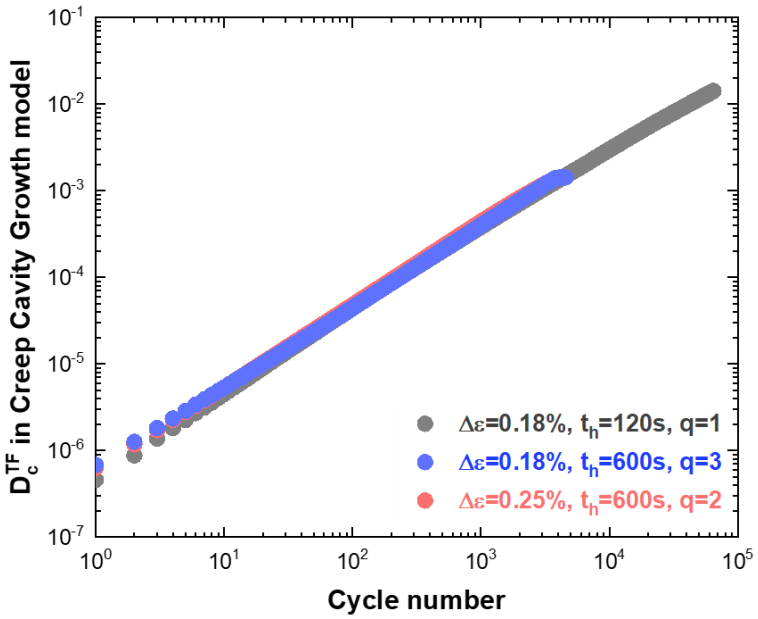

Figure 6. Accumulated creep damage calculated using the creep cavity growth model as a function of applied cycles for the standard CF test with 120 s tensile hold at 0.18% strain range and SMT-based CF with 600 s tensile hold and elastic follow-up factor of 2 at 0.25% strain range and an elastic follow-up factor of 3 at 0.18% strain range.

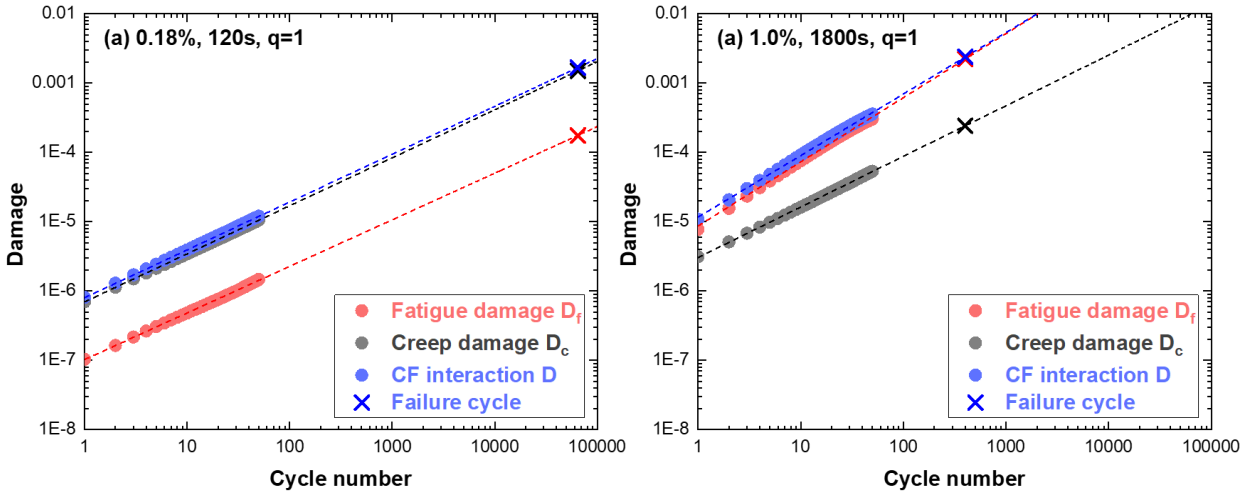

Figure 7. Creep damage, fatigue damage, and CF interactive damage calculated by the Time Fraction method for the standard CF test at strain ranges of (a) 0.18% (low strain range) and (b) 1.0% (high strain range) with 120 s and 1800 s hold times, respectively.

5.1.2 Damage Evolution Using Dissipated Energy Method

The creep damage evolution calculated using the deformation equations in *Section 4.2* using the Dissipated Energy method are presented in this section. The available CF failure data with strain ranges of 0.3%, 0.6%, and 1.0% and relatively short hold times of 180 s, 600 s, 1,800 s, and 9,000 s were analyzed, and the accumulated creep damages as a function of applied cycles are plotted in Figure 8. The results show that the damages also have a power-law relationship to the cycle number and that the damages are quite comparable regardless of the tensile hold times. This finding is consistent with relevant studies on the tensile-hold CF testing showing that CF failure life cycles are not significantly reduced even though the hold time increases.

Figure 9 shows the accumulated creep damage evolution as a function of cycle of standard 120 s tensile-hold CF failure data at 0.18% strain range and SMT 600 s tensile-hold CF failure data with and elastic follow-up factor of 2 0.25% and an elastic follow-up factor of 3 at 0.18% strain range, respectively. It can be found that the accumulated creep strain energy at material failure at relatively low strain ranges of 0.3%, 0.25%, and 0.18% is comparable and stays at about 150 mJ/mm^3. Note that this value at failure is higher than that at high strain range ranges.

For prediction of CF life cycles with longer hold times, it is assumed that the stress relaxation behavior is controlled by power-law creep (i.e., $A = 0$ in Eq. 4). The stress exponent n in the power-law creep relationship used the same value of 5.6 (Benz et al. 2014). Figure 10 presents the accumulated creep damage with extended hold times. The creep damage becomes saturated when the hold time is increased to 10 h.

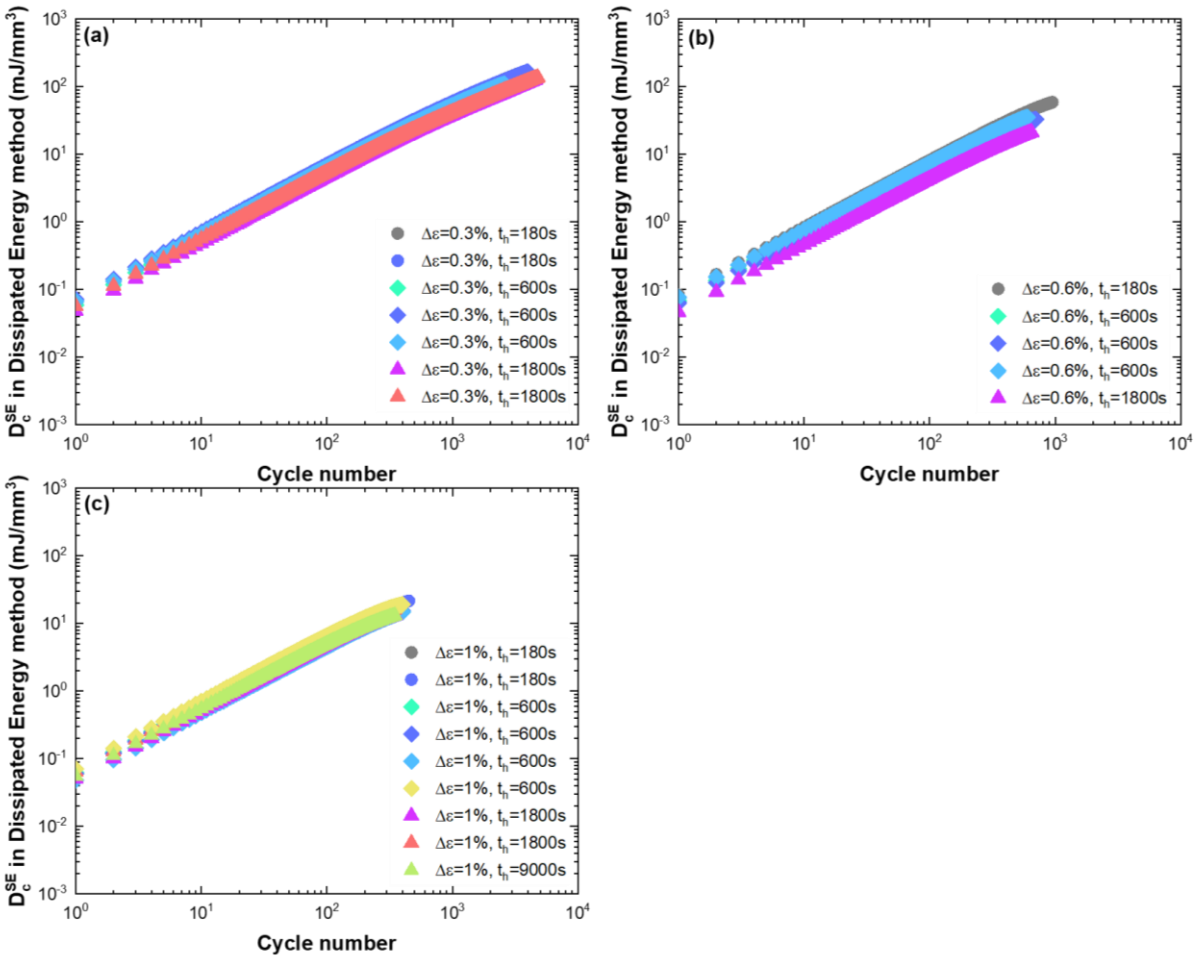

Figure 8. Accumulated creep damage at strain ranges of (a) 0.3%, (b) 0.6%, and (c) 1.0% with tensile hold times of 180 s, 600 s, 1,800 s, and 9,000 s as a function of applied cycle.

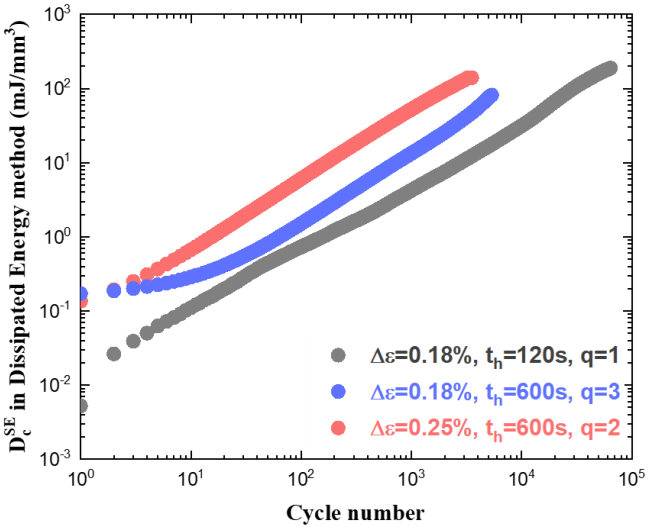

Figure 9. Accumulated creep damage calculated using the Dissipated Energy method as a function of applied cycles for the standard 120 s tensile hold CF test at 0.18% strain range and the SMT-based CF test with 600 s tensile hold and an elastic follow-up factor of 2 at 0.25% strain range and an elastic follow-up factor of 3 at 0.18% strain range.

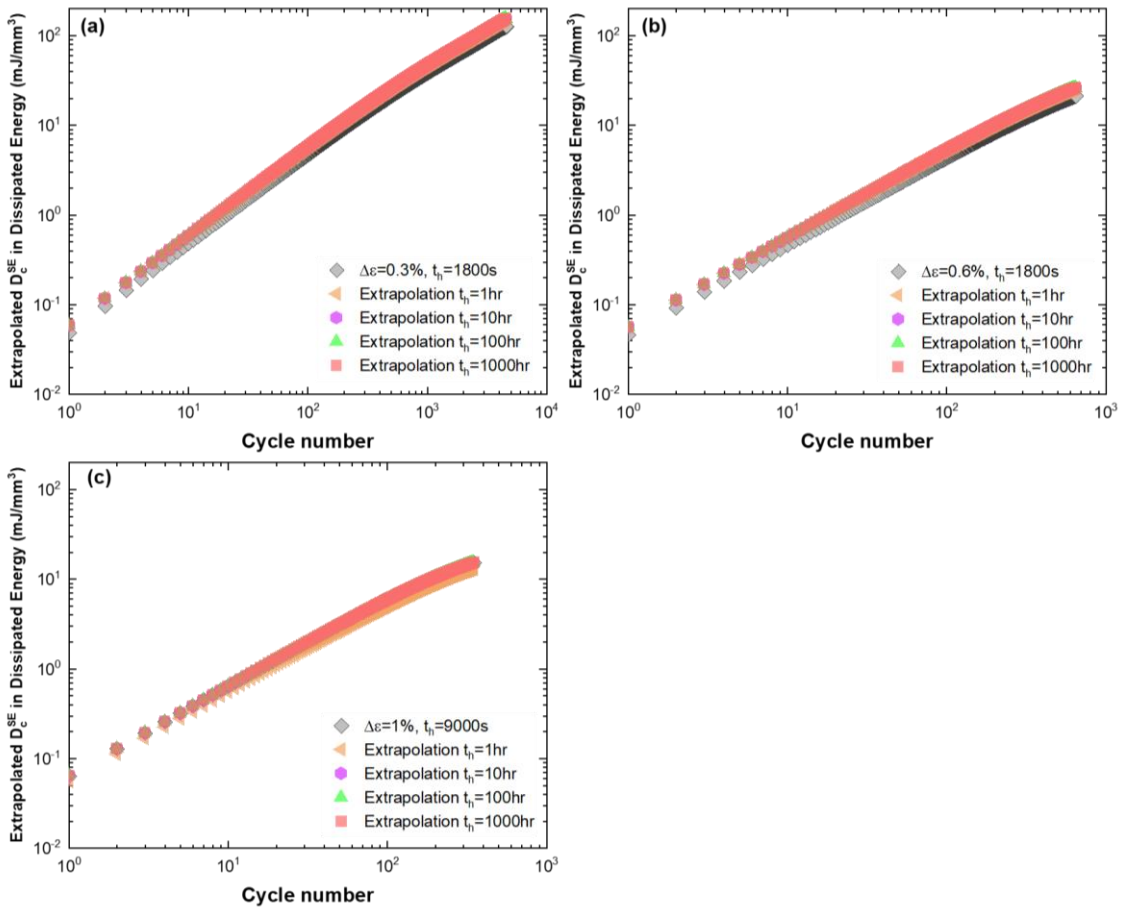

Figure 10. Extrapolated creep damage accumulation curves to longer hold times at strain ranges of 0.3%, 0.6%, and 1.0% with tensile hold times of 180 s; 600 s; 1,800 s; and 9,000 s as a function of applied cycle.

Figure 11 shows the fatigue damage evolution of CF failure data at high strain ranges (i.e., 0.3%, 0.6%, and 1.0%) calculated using Dissipated Energy method. Similarly, the fatigue damage does not vary significantly with hold times, indicating a saturated influence of hold time on fatigue damage. This analysis indicates that the experimental CF life curve measured at high strain ranges with relatively short hold time is sufficient to estimate the CF life at high strain ranges with extended hold times in the Dissipated Energy method. In this study, the lowest value of creep damage assessed using Dissipated Energy method from CF failure data is later used to perform CF life prediction at low strain ranges.

At low strain ranges, the creep damage is assumed to be the dominating factor for material failure (Hales, 1980). In analysis, the accumulated fatigue damage, D_f^{SE}, is set to be zero when the strain range is less than 0.3%, and creep damage is analyzed to predict CF life at low strain ranges of less than 0.3%.

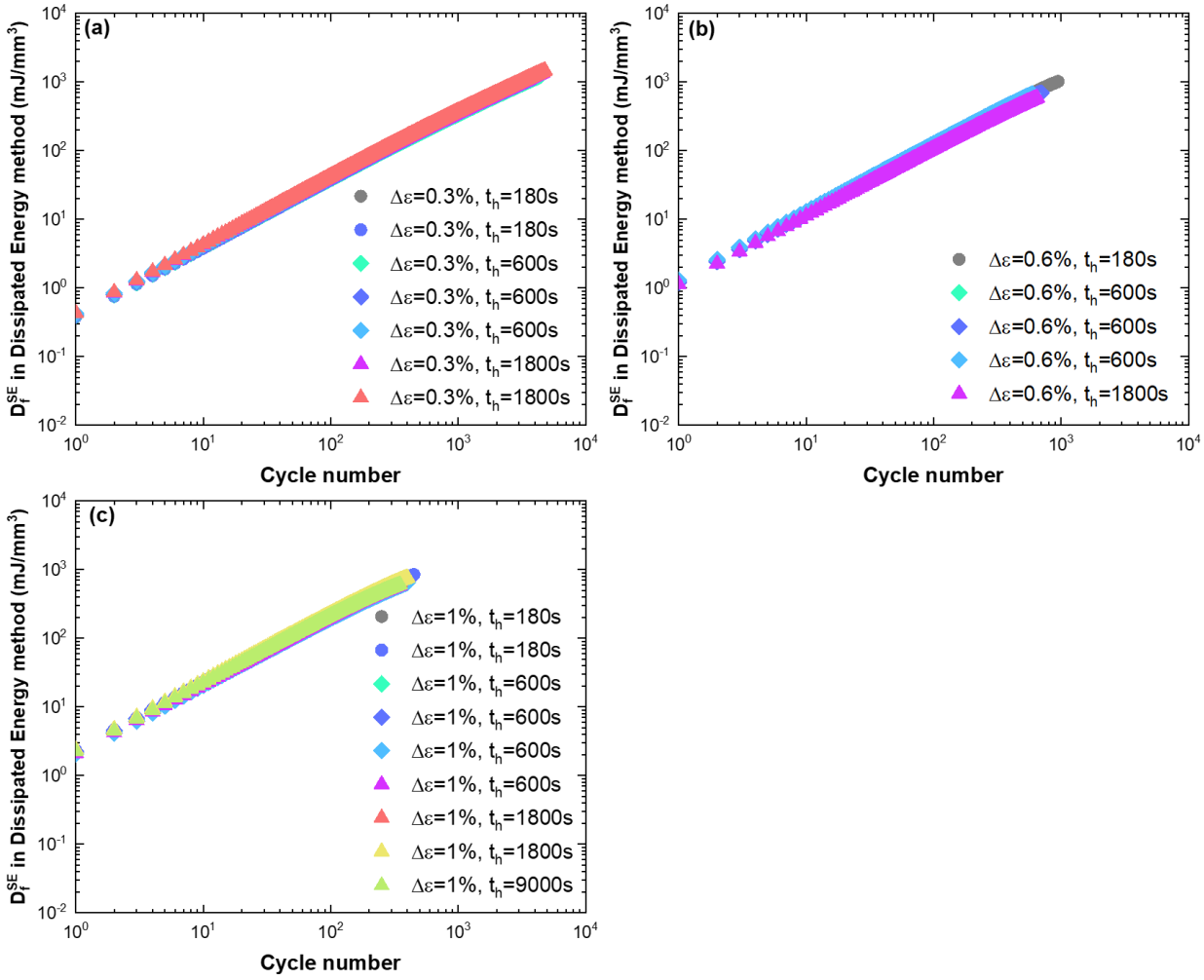

Figure 11. Accumulated fatigue damage calculated using Dissipated Energy method at strain ranges of 0.3%, 0.6%, and 1.0% with tensile hold time of 180 s; 600 s; 1,800 s and 9,000 s as a function of applied cycle.

6. PREDICTION ON CREEP-FATIGUE LIFE CYCLES

The predicted representative tensile hold CF life cycles for Alloy 617 at 950ºC are presented in Figure 12 using the Time Fraction method. The available CF failure data are also plotted in the figure. Figure 12a shows the results of the standard CF test with an elastic follow-up factor of 1, and the hold time is extrapolated to 100 h and the strain range to 0.1%. Figure 12b shows the CF life curves having 600 s tensile hold time of SMT CF tests with elastic follow-up factors of 2 and 6. As the hold time increases, the life decreases in this Time Fraction method. The CF life curves were generated using these predicted life cycles at different strain ranges.

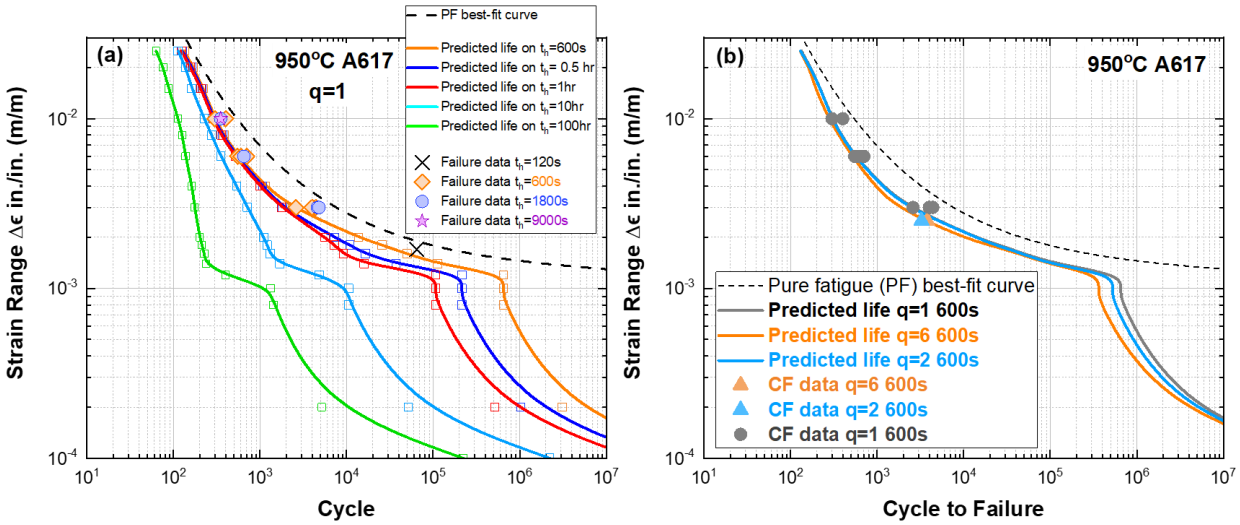

Figure 12. Representative tensile-hold CF life curves with an elastic follow-up factor of (a) q=1 and (b) q=2 and 6 for Alloy 617 at 950°C using the Time Fraction method

Figure 13 shows the representative tensile-hold CF life curves predicted using the Dissipated Energy method with elastic follow-up factor of 1. As described in *Section 5.1.2*, an increased hold time does not significantly affect the CF life because the changes in the stress rate or creep strain rate are extremely small when holding exceeds a certain amount of time. Therefore, the previously reported best-fit curves with short hold time of 0.5 hr at the strain range of 0.3% and above are used to predict CF life with longer hold times. The experimental data from the specially designed block-strain range CF tests are used to predict the CF life cycles and longer hold times at low strain ranges.

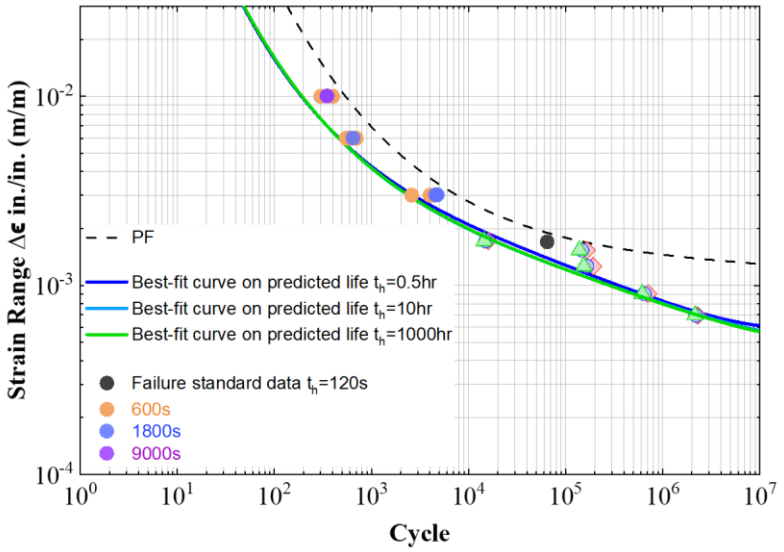

Figure 13. Representative standard tensile-hold CF life curves predicted using the Dissipated Energy method.

7. EXPERIMETAL VERIFICATION OF THE CF LIFE PREDICTION

Comparison of CF life prediction using the Time Fraction and Dissipated Energy method shows different results, especially at low strain ranges and long hold times. To verify the predicted CF life on Alloy 617 at low strain ranges and long hold times, while providing a better understanding and assessment of CF damage, a SMT-based CF test with an elastic follow-up factor of 3 was designed and is being performed to verify the CF prediction. Considering the accumulated CF damaging interaction as the key parameter controlling the material failure and test duration, this designed test was first carried out for 900 cycles at a strain range of 0.4% with 180 s tensile hold to accumulate about 80% CF damage, calculated based on the Time Fraction method. Subsequently, CF continues on the same specimen and is subjected to CF loading at low strain range of 0.2% with 10 hr tensile hold time for the remaining ~20% of CF life.

The test design is illustrated in Figure 14, along with the predicted CF curves. This experimental approach significantly reduces the test duration and produces a test to failure at low strain range.

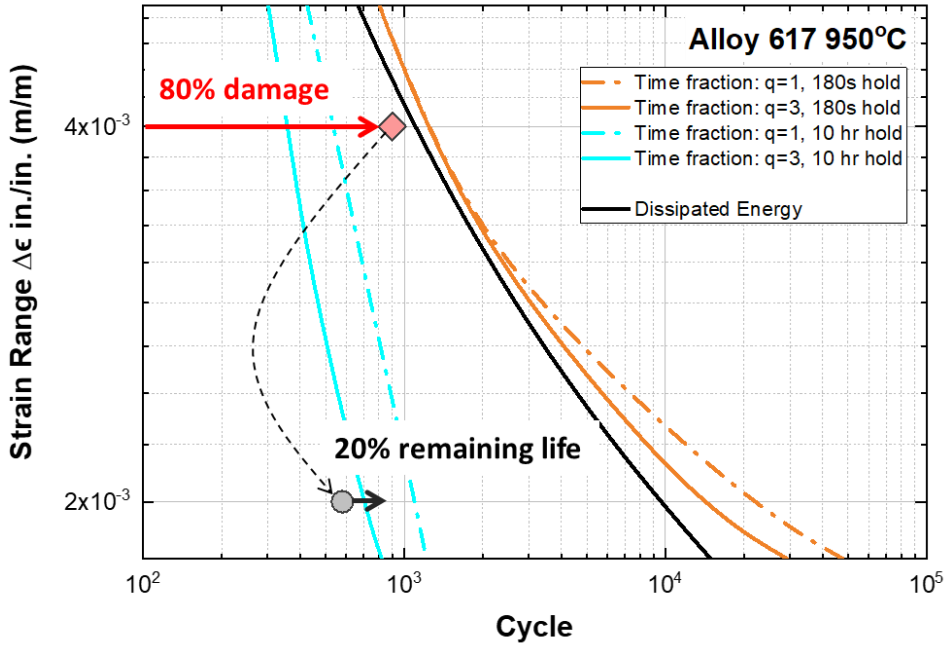

Figure 14. Illustration of specially designed CF test for verifying the CF life prediction on Alloy 617 at 950°C.

This SMT-based verification testing is on-going. The first step with loading at a strain range of 0.4% with 180 s tensile hold has been completed. Figure 15 shows the hysteresis hoops of the representative cycles and the maximum and minimum stresses evolutions. The second step at low strain range of 0.2% with a 10 hr tensile hold time is on-going and accumulated 90 of cycles while this report is written. The goal is to test the specimen to failure and provide the test verification for CF life prediction.

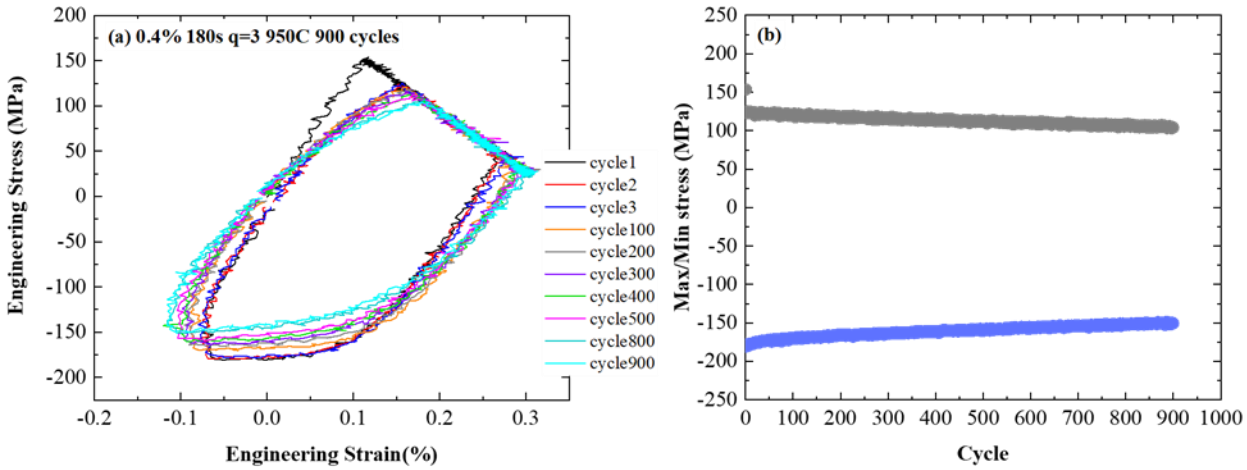

Figure 15. (a) Hysteresis hoops and (b) the maximum and minimum stress evolutions of specially designed CF testing for 80% CF damage accumulation (900 cycles) at 0.4% strain range with a 180 s tensile hold and elastic follow-up factor of 3.

8. SUMMARY

The lack of test data in the high cycle and low strain range region is a critical issue in finalizing the EPP+SMT CF design curves. The limitations in experimental data at low strain ranges and long hold times are due to extraordinarily long failure times at the small strain ranges and the inability of the test machine to control these small strain ranges because of the signal-to-noise issues.

In this work, available CF data with failure cycles at different strain ranges were analyzed and used to assess two general damage evaluation methods in predicting CF life cycles: the Time Fraction method and the Dissipated Energy method. The results show that it is possible to use a limited number of testing cycles to predict CF life cycles through the development of a physics-based extrapolation approach. Specifically designed experiments using the proposed block-strain range CF testing method were performed with standard strain-controlled CF in generating the critical information needed to calibrate material parameters and extrapolate CF data to low strain ranges and long hold times. Based on this new testing approach, preliminary EPP+SMT CF life curves were developed for Alloy 617 at 950°C with different tension hold times.

Additionally, a SMT-based test was designed and is being performed to verify the EPP+SMT CF fatigue curves generated using the predicted CF life cycles. In FY2023, the extrapolation procedure will be applied at lower temperatures. The strain range will be correlated to the strain ranges calculated using the EPP method to complete the development of the EPP+SMT CF design curves for Alloy 617. Critical experiments are expected to be performed for verification purpose.

.

REFERENCE

ASMT E2714, “Standard Test Method for Creep-Fatigue Testing”, ASTM International, West Conshohocken, PA.

ASTM-E606, “Standard Test Method for Strain-Controlled Fatigue Testing”, ASTM International, West Conshohocken, PA.

Barua, B, Messner, M.C., Sham, T.-L., Jetter, R. I., Wang, Y., (2020), "Preliminary description of a new creep-fatigue design method that reduces over conservatism and simplifies the high temperature design process", ANL-ART-194, Argonne National Laboratory, Lemont, IL.

Barua, B, Messner, M.C., Wang, Y., Sham, T.-L., Jetter, R. I. (2021), "Draft Rules for Alloy 617 Creep-Fatigue Design using an EPP+SMT Approach", ANL-ART-227, Argonne National Laboratory, Lemont, IL

Benz, J. K., Carroll, L. J., Wright, J. K., Wright, R. N., & Lillo, T. M. (2014). “Threshold stress creep behavior of alloy 617 at intermediate temperatures”. Metallurgical and Materials Transactions A, 45(7), 3010-3022.

Kobatake, K., Ohta, H., Ishiyama, H., Kaihara, T. and Ueno, O. (1999). “An alternate approach to creep-fatigue damage with elastic follow-up for high temperature structural design”. Journal of national fisheries university, 48(1), pp.25-39.

Cocks, A. C. F., & Ashby, M. F. (1982). “On creep fracture by void growth. Progress in materials science”, 27(3-4), 189-244.

Frost, Harold J., and Michael F. Ashby (1982). “Deformation mechanism maps: the plasticity and creep of metals and ceramics”. Pergamon press.

Chaboche, J.L. (1989). “Constitutive equations for cyclic plasticity and cyclic viscoplasticity. International journal of plasticity”, 5(3), pp.247-302.

Zhao, L., Xu, L., Han, Y., Jing, H. and Gao, Z. (2019). “Modelling creep-fatigue behaviours using a modified combined kinematic and isotropic hardening model considering the damage accumulation”, International Journal of Mechanical Sciences, 161, p.105016.

Li, Z., Kiran, R., Hu, J., Hector, L.G. and Bower, A.F. (2020). “Analysis and design of a three-phase TRIP steel microstructure for enhanced fracture resistance”. International Journal of Fracture, 221(1), pp.53-85.

Hales, R.,(1980), “A Quantitative Metallographic Assessment of Structural Degradation of Type 316 Stainless Steel during Creep-Fatigue”, Vol. 3, No. 4, pp. 339-356, Fatigue of Engineering Materials and Structures.

Ostergren, W. J. (1976). “A damage function and associated failure equations for predicting hold time and frequency effects in elevated temperature, low cycle fatigue. Journal of Testing and Evaluation”, 4(5), 327-339.

Manson, S. S. and Zab, R.,, (1977), “Treatment of Low Strains and Long Hold Times in High Temperature Metal Fatigue by Strain Range Partitioning”, ORNL/sub-3988/1, Oak Ridge National Laboratory, Oak Ridge, TN.

Messner, M. C., Sham, T. L., Wang, Y., and R. I. Jetter, R.I. (2018), “Evaluation of methods to determine strain ranges for use in SMT design curves”, ANL-ART-138, Argonne National Laboratory, Lemont, IL.

Sham, T. L., & Needleman, A. (1983). “Effects of triaxial stressing on creep cavitation of grain boundaries”. Acta Metallurgica, 31(6), 919-926.

Skelton, R.P. and Gandy, D. (2008). “Creep–fatigue damage accumulation and interaction diagram based on metallographic interpretation of mechanisms”. Materials at High Temperatures, 25(1), pp.27-54.

Wang, Y., Jetter, R. I., Krishnan, K., and Sham, T.-L (2013) “Progress Report on Creep-Fatigue Design Method Development Based on SMT Approach for Alloy 617”, ORNL/TM-2013/349, Oak Ridge National Laboratory, Oak Ridge, TN.

Wang, Y., Jetter, R. I. and Sham, T.-L (2014), “Application of Combined Sustained and Cyclic Loading Test Results to Alloy 617 Elevated Temperature Design Criteria”, ORNL/TM-2014/294, Oak Ridge National Laboratory, Oak Ridge, TN.

Wang, Y., Jetter, R. I., Baird, S. T., Pu, C. and Sham, T.-L. (2015), “Report on FY15 Two-Bar Thermal Ratcheting Test Results”, ORNL/TM-2015/284, Oak Ridge National Laboratory, Oak Ridge, TN.

Wang, Y., Jetter, R. I., and Sham, T.-L. (2016a), “FY16 Progress Report on Test Results In Support Of Integrated EPP and SMT Design Methods Development” ORNL/TM-2016/330, Oak Ridge National Laboratory, Oak Ridge, TN.

Wang, Y., Jetter, R. I., and Sham, T.-L. (2016b), “Preliminary Test Results in Support of Integrated EPP and SMT Design Methods Development”, ORNL/TM-2016/76, Oak Ridge National Laboratory, Oak Ridge, TN.

Wang, Y., Jetter, R.I., and Sham, T.-L. (2017a), “Report on FY17 Testing in Support of Integrated EPP-SMT Design Methods Development”, ORNL/TM-2017/351, Oak Ridge National Laboratory, Oak Ridge, TN.

Wang, Y., Jetter, and Sham, T.-L. (2017b), “Pressurized Creep-Fatigue Testing of Alloy 617 Using Simplified Model Test Method”, Proceedings of the ASME 2017 Pressure Vessels and Piping Conference, PVP2017-65457, American Society of Mechanical Engineers, New York, NY.

Wang, Y., Jetter, R. I., Messner, M., Mohanty, S., and Sham, T.-L. (2017c), “Combined Load and Displacement Controlled Testing to Support Development of Simplified Component Design Rules for Elevated Temperature Service”, Proceedings of the ASME 2017 Pressure Vessels and Piping Conference, PVP2017-65455, American Society of Mechanical Engineers, New York, NY.

Wright, J. K., et al. "Determination of the creep-fatigue interaction diagram for Alloy 617", Pressure Vessels and Piping Conference. Vol. 50411. American Society of Mechanical Engineers, 2016.

Wang, Y., Jetter, R. I., Messner, M., and Sham, T.-L. (2018), “Report on FY18 Testing Results in Support of Integrated EPP-SMT Design Methods Development”, ORNL/TM-2018/887, Oak Ridge National Laboratory, Oak Ridge, TN.

Wang, Y., Jetter, R. I., Messner, M., and Sham, T.-L. (2019), “Development of Simplified Model Test Method for Creep-fatigue Evaluation”, Proceedings of the ASME 2019 Pressure Vessels and Piping Conference, PVP2019-93648, American Society of Mechanical Engineers, New York, NY.

Wang, Y., Hou, P., Jetter, R. I., and Sham, T.-L. (2020), “Report on FY2020 Test Results in Support of the Development of EPP Plus SMT Design Method”, ORNL/TM-2020/1620, Oak Ridge National Laboratory, Oak Ridge, TN.

Wang, Y., Hou, P., Jetter, R. I., and Sham, T.-L. (2021), “Evaluation of the Primary-Load Effects on Creep-Fatigue Life of Alloy 617 Using Simplified Model Test Method”, Proceedings of the ASME 2021 Pressure Vessels and Piping Conference, PVP2021-61658, American Society of Mechanical Engineers, New York, NY

Wang, Y., Hou, P., Jetter, R. I., and Sham, T.-L. (2021), "Report on FY2021 Test Results in Support of the Development of EPP Plus SMT Design Method", ORNL/TM-2021/2159, Oak Ridge National Laboratory, Oak Ridge, TN.

Wang, Y. (2022), "Alternative Creep-Fatigue Design Method Using EPP+SMT", Advanced Reactor Technologies Program, Advanced Materials R&D Program Review, Virtual meeting.

Wright, J. K., Carroll, L. J., Sham, T. L., Lybeck, N. J., & Wright, R. N. (2016). "Determination of the creep-fatigue interaction diagram for Alloy 617". In Pressure Vessels and Piping Conference (Vol. 50411, p. V005T12A004). American Society of Mechanical Engineers.